

Pentagram Integrals and Poncelet Families

Richard Evan Schwartz *

April 25, 2010

1 Introduction

This paper concerns the behavior of the monodromy invariants of the pentagram map, as applied to Poncelet polygons. This paper is really part of a larger project, joint with Valentin Ovsienko and Sergei Tabachnikov, to understand the structure of the pentagram map. In particular, we hope to find an easy geometric fact of the theorem I establish in this paper.

A *Poncelet polygon* is a polygon that has all vertices on one conic and all edges tangent to another conic. Two Poncelet n -gons lie in the same Poncelet family iff their points lie on the same conic C_1 , and their edges are tangent to the same conic C_2 . (We sometimes say that these two polygons are *related*.) In general, each Poncelet polygon includes in a 1-parameter family of Poncelet polygons lying on the same family. This is the content of the famous Poncelet porism. Here is the main result.

Theorem 1.1 *Any two related Poncelet polygons have the same monodromy invariants. In other words, the monodromy invariants are constant on Poncelet families.*

We spend the rest of the introduction describing what we mean by the *monodromy invariants*.

First of all, we discuss the pentagram map. The pentagram map is a geometric iteration defined on polygons. This map is defined in practically any

* Supported by N.S.F. Research Grant DMS-0072607 and also a Clay Research Scholarship

field, but it is most easily described for polygons in the real projective plane. Geometrically, the pentagram map carries the polygon P to the polygon Q , as shown in Figure 1. The labelling is transferred from P to Q in the obvious way.

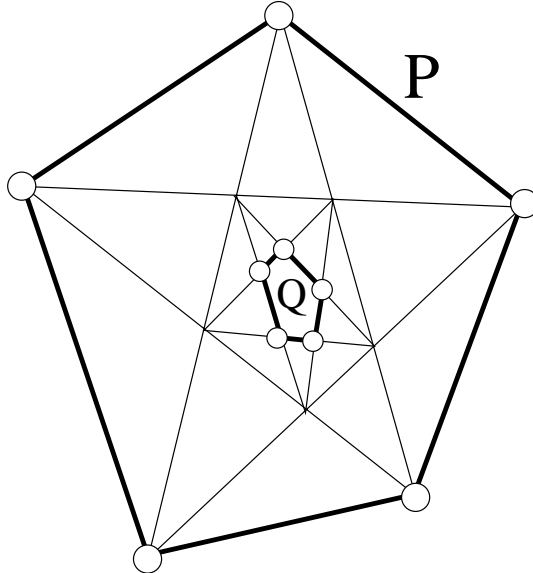


Figure 1: The pentagram map

This map is always defined for convex polygons, and generically defined for all polygons. The pentagram map commutes with projective transformations and induces a generically defined map T on the space \mathcal{Q}_n of cyclically labelled n -gons modulo projective transformations. T is the identity map on \mathcal{Q}_5 and has period 2 on \mathcal{Q}_6 . The map T is not periodic on \mathcal{Q}_n for $n \geq 7$.

The pentagram map also defines a map on a slightly larger space \mathcal{P}_n . The space \mathcal{P}_n is the space of *twisted n -gons* mod projective transformations. A twisted n -gon is a map $\phi : \mathbf{R} \rightarrow \mathbf{RP}^2$, such that

$$\phi(k+n) = M \circ \phi(k) \quad \forall k. \quad (1)$$

Here M is a real projective transformation, called the *monodromy* of the twisted polygon. The space \mathcal{P}_n contains the space \mathcal{Q}_n as a codimension 8 submanifold.

This pentagram map is studied for pentagons in [M]. We studied the general case in [S1], [S2], and [S3]. Finally, in [OST] we showed that the

pentagram map is a completely integrable system on \mathcal{P}_n . We think that the pentagram map is a completely integrable system on \mathcal{Q}_n as well, but there are certain technical details we need to resolve before establishing this fact.

In [S3] we constructed polynomial functions

$$O_1, \dots, O_{[n/2]}, O_n, E_1, \dots, E_{[n/2]}, E_n : \mathcal{P}_n \rightarrow \mathbf{R} \quad (2)$$

which are invariant under the pentagram map. In [OST] these functions are recognized a complete list of integrals for the completely integrable system. There is an invariant Poisson structure, and the above functions Poisson-commute with respect to this Poisson structure. We call these functions the *monodromy invariants*, and we will construct them in the next section.

Our main result says that each function O_k and E_k is constant when restricted to a Poncelet family. Here $k = 1, \dots, [n/2], n$. For convenience, we will prove this result for n even. The odd case has a similar proof. Our proof is really an argument in complex analysis. When defined over \mathbf{C} , the generic Poncelet family is naturally parametrized by a complex torus \mathbf{T} . The monodromy functions are meromorphic functions on \mathbf{T} , and our goal is to show that these functions are all constant. Our technique is to analyze the potential poles of the functions, which correspond to the singular Poncelet polygons within the family. We show that the functions are all bounded in neighborhoods of the singular Poncelet polygons, thereby showing that there are no poles at all. Consequently, all the functions must be constant.

Here is an overview of the paper. In §2, we will define the monodromy invariants. In §3, we give an overview of the proof, reducing Theorem 1.1 to two main technical lemmas, Lemma 3.3 and Lemma 3.4. In §4 we prove a technical result about degenerating pentagons. This result will be useful for the proof of Lemma 3.4. In §5 we recall the complex-torus picture associated to a Poncelet family. In §6 we give a model for the way the Poncelet polygons degenerate as we approach a singular point on the complex torus. In §7 we prove Lemma 3.3. In §8-10 we prove Lemma 3.4.

I'd like to thank Sergei Tabachnikov and Valentin Ovsienko for many interesting and helpful discussions about the pentagram map. I would also like to thank the IHES and Caltech for their support during the writing of this paper.

2 The Monodromy Invariants

The papers [S3] and [OST] give a good account of the monodromy invariants. The notation in the two papers is slightly different, and we will follow [OST]. First of all, we have the *cross ratio*

$$[t_1, t_2, t_3, t_4] = \frac{(t_1 - t_2)(t_3 - t_4)}{(t_1 - t_3)(t_2 - t_4)}. \quad (3)$$

Suppose that ϕ is a twisted n -gon, with monodromy M . We let ¹ $v_i = \phi(i)$. The label i in Figure 2 denotes v_i , and similarly for the other labels.

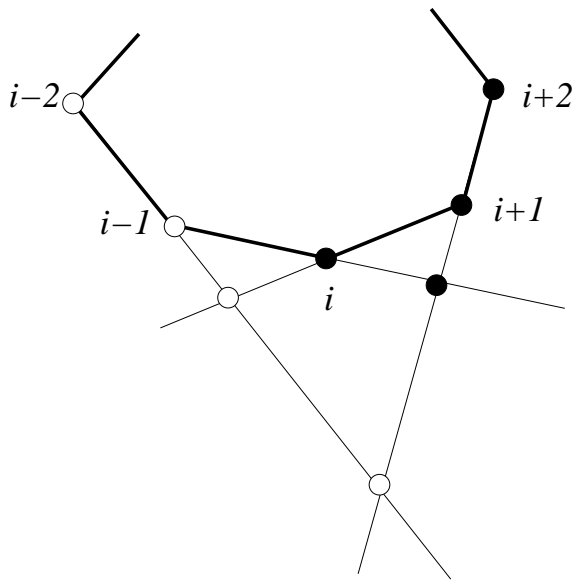


Figure 2: vertex labels

We associate to each vertex v_i two numbers:

$$\begin{aligned} x_i &= [v_{i-2}, v_{i-1}, ((v_{i-2}, v_{i-1}) \cap (v_i, v_{i+1})), ((v_{i-2}, v_{i-2}) \cap (v_{i+1}, v_{i+2}))] \\ y_i &= [v_{i+2}, v_{i+1}, ((v_{i+2}, v_{i+1}) \cap (v_i, v_{i-1})), ((v_{i+2}, v_{i+2}) \cap (v_{i-1}, v_{i-2}))] \end{aligned} \quad (4)$$

Here (a, b) denotes the line determined by points a and b . Here, for instance, x_i is the cross ratio of the 4 white points in Figure 2. We call the invariants $x_1, y_1, x_2, y_2, \dots$ the *corner invariants*. These invariants form a periodic sequence of length $2n$. That is $x_{k+n} = x_k$ and $y_{k+n} = y_k$ for all k .

¹Later on, it will be convenient to change our notation, so that $V(i) = \phi(i)$.

We define

$$O_n = \prod_{i=1}^n x_i; \quad E_n = \prod_{i=1}^n y_i. \quad (5)$$

The other monodromy invariants are best defined in an indirect way. Recall that M is the monodromy of our twisted polygon ϕ . We lift M to an element of $GL_3(\mathbf{R})$ which we also denote by M . We define

$$\Omega_1 = \frac{\text{trace}^3(M)}{\det(M)}; \quad \Omega_2 = \frac{\text{trace}^3(M^{-1})}{\det(M^{-1})}. \quad (6)$$

These quantities are independent of the lift of M and only depend on the conjugacy class of M . Finally, these quantities are invariant under the pentagram map.

We define

$$\tilde{\Omega}_1 = O_n^2 E_n \Omega_1; \quad \tilde{\Omega}_2 = O_n E_n^2 \Omega_2. \quad (7)$$

It turns out that these quantities are polynomials in the corner invariants. The remaining monodromy invariants are suitably weighted homogeneous parts of these polynomials.

We have a basic rescaling operation

$$R_t(x_1, y_1, x_2, y_2, \dots) = (tx_1, t^{-1}y_1, tx_2, t^{-1}y_2, \dots). \quad (8)$$

We say that a polynomial in the corner invariants has *weight* k if

$$R_t^*(P) = t^k P. \quad (9)$$

Here R_t^* denotes the obvious action of R_t on polynomials. In [S3] we show that

$$\tilde{\Omega}_1 = \sum_{k=1}^{n/2} O_k; \quad \tilde{\Omega}_2 = \sum_{k=1}^{n/2} E_k. \quad (10)$$

Here n is even. This sum defines the remainder of the monodromy invariants. These polynomials have explicit formulas, also worked out in [S3] and [OST], but we don't need these formulas for our purposes here.

3 Overview of the Proof

We will deduce Theorem 1.1 from two lemmas. The first lemma is a special case of Theorem 1.1.

Lemma 3.1 $E_n(P') = E_n(P)$ and $O_n(P) = O_n(P)$.

The second lemma involves the scaling operation we mentioned above. For $t \in \mathbf{R}$, let P_t denote the twisted n -gon with invariants

$$\dots tx_0, t^{-1}x_1, tx_2, t^{-1}x_3, \dots,$$

normalized so that $V_t(j) = V(j)$ for $j = 1, 2, 3, 4$. Here $V(j)$ is the j th vertex of P and $V_t(j)$ is the j th vertex of P_t .

Lemma 3.2 *There are infinitely many values t for which $\Omega_1(P_t) = \Omega_1(P')$ and $\Omega_2(P_t) = \Omega_2(P')$.*

Proof of Theorem 1.1: Let t be any of the values from Lemma 3.2. We have the general homogeneity relations:

$$E_k(P_t) = t^k E_k(P); \quad O_k(P_t) = t^{-k} O_k(P). \quad (11)$$

Lemma 3.1 combines with Equation 11 to give

$$E_n(P_t) = E_n(P'); \quad O_n(P_t) = O_n(P'). \quad (12)$$

Combining Equations 10, Equation 11, Equation 12, and Lemma 3.2, we have

$$\sum_{k=1}^{n/2} t^k (E_k(P) - E_k(P')) = 0, \quad (13)$$

for all t near 1. But then we have a polynomial with infinitely many roots. Hence, all the coefficients are 0. That is, $E_k(P) = E_k(P')$ for all k . Similarly $O_k(P) = O_k(P')$ for all k . ♠

We will prove Lemmas 3.1 and 3.2 by the same technique, which we now describe. The idea is to complexify. Over \mathbf{C} , the set of Poncelet polygons related to P is parametrized by a complex torus \mathbf{T} . One identifies the points on \mathbf{T} with *flags* (p, L) , where $p \in C_1$ and L is a line through p and tangent

to C_2 . There are two kinds of Poncelet polygons in this family, *ordinary* and *degenerate*. The ordinary Poncelet polygons are those consisting of n distinct points in general position. The rest of the polygons we call *degenerate*. (Below we will analyze the structure in detail.) We classify the points of \mathbf{T} as *ordinary* and *degenerate*, according to the type of polygon they correspond to. There are finitely many degenerate points.

Let $f : \mathbf{T} \rightarrow \mathbf{C}$ denote the function $f(z) = E_n(P^z)$. Here P^z is the Poncelet polygon whose 1st and 2nd vertices determine the flag associated to z . The vertex of the flag is $V^z(1)$ and the line contains $V^z(1)$ and $V^z(2)$. The function f is a *rational function* on \mathbf{T} . By this we mean that f is holomorphic away from the degenerate points of T , and f has a Laurent series in the neighborhood of each degenerate point. That is, f has no essential singularities. We will prove the following result.

Lemma 3.3 *For each degenerate point $z \in \mathbf{T}$ there is a sequence $\{z_j\}$ of ordinary points such that $z_j \rightarrow z$ and $\{f(z_j)\}$ is bounded.*

Since f is a rational function, Lemma 3.3 implies that f has no poles on \mathbf{T} . Hence f is constant. This proves Lemma 3.1.

We will take a similar approach to Lemma 3.2. There is an action of D_n , the order $2n$ dihedral group, on \mathbf{T} , such that the orbits are exactly the flags corresponding to Poncelet polygons. We describe this action below in detail. We call two points of \mathbf{T} *equivalent* if they are in the same D_n orbit.

Lemma 3.4 *For each degenerate point z' there is an equivalent degenerate point z with the following property. If t is sufficiently close to 1 then there is a sequence $\{z_j\}$, converging to z , such that*

- $P_t^{z_j}$ exists.
- $\lim_{j \rightarrow \infty} P_t^{z_j}$ is a well-defined twisted n -gon.

Let $g_t(z) = \Omega_1(P_t^z)$ and $h_t(z) = \Omega_2(p_t^z)$. Lemma 3.4 covers one degenerate point per equivalence class. Lemma 3.4 says that the functions g_t and h_t have no poles at our special points. But the unordered pair $\{g_t, h_t\}$ is constant on D_n -orbits. Hence, g_t and h_t have no poles at all. Hence, these functions are constant. This proves Lemma 3.2.

The rest of the paper is devoted to proving Lemmas 3.3 and 3.4.

4 Variation of Pentagons

Here we establish a technical result about the corner invariants of a degenerating pentagon. We now consider a family $\{P_n\}$ of pentagons with t a parameter near 1. Recall that $x_1, y_1, \dots, x_5, y_5$ are the corner invariants.

Lemma 4.1 *Let P be a strictly convex pentagon and let $\{P_n\}$ be a sequence of strictly convex pentagons such that*

1. $V_n(k) \rightarrow V(k)$ for $k = 1, 2, 3, 4$.
2. $x_1(P_n) \rightarrow x_1(P)$
3. $y_5(P_n) \rightarrow y_5(P)$

Then $V_n(5) \rightarrow V(5)$

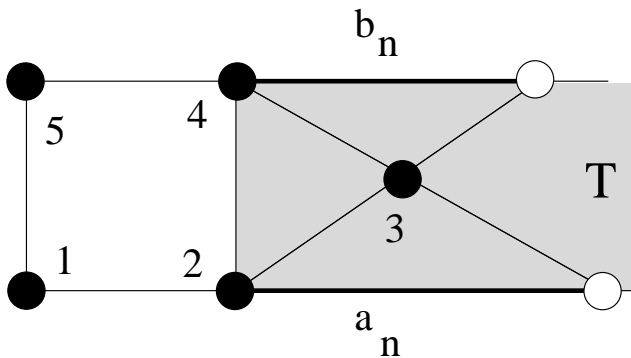


Figure 3: compactness argument

Proof: We normalize so that the vertices $V(1), V(2), V(4), V(5)$ are the vertices of a unit square, as in Figure 3. Let T_n be a projective transformation such that $T_n(V_n(k)) = V(k)$ for $k = 1, 2, 4, 5$. Referring to Figure 3, we have

$$a = x_1; \quad b = y_5$$

But a and b determine the location of $V(3)$. From these facts, and from our hypotheses, we see that $T_n(V_n(3)) \rightarrow V(3)$.

Now we see that $V_n(k) \rightarrow V(k)$ for $k = 1, 2, 3, 4$ and $T_n(V_n(k)) \rightarrow V(k)$ for $k = 1, 2, 3, 4$. Since these points are all in general position, this forces $T_n \rightarrow I$, the identity transformation. Hence $P_n \rightarrow P$. ♠

5 The Complex Picture

The complex torus \mathbf{T} arises in the proof of the Poncelet porism. For $j = 1, 2$ we have maps $\phi_j : \mathbf{T} \rightarrow C_j$ given by

$$\phi_1(z) = p; \quad \phi_2(z) = L \cap C_2; \quad z = (p, L). \quad (14)$$

Both ϕ_1 and ϕ_2 are double branched-covers. The map ϕ_1 is branched over the 4 points of $C_1 \cap C_2$. The map ϕ_2 is branched over the points of $x \in C_2$ such that the line tangent to C_2 at x is also tangent to C_1 . There are 4 such points.

There is some real plane $X \subset \mathbf{CP}^2$ such that $C_1 \cap C_2 \subset X$, and also all common tangent lines lie in X . We can identify X with \mathbf{R}^2 . The picture then looks like Figure 4.

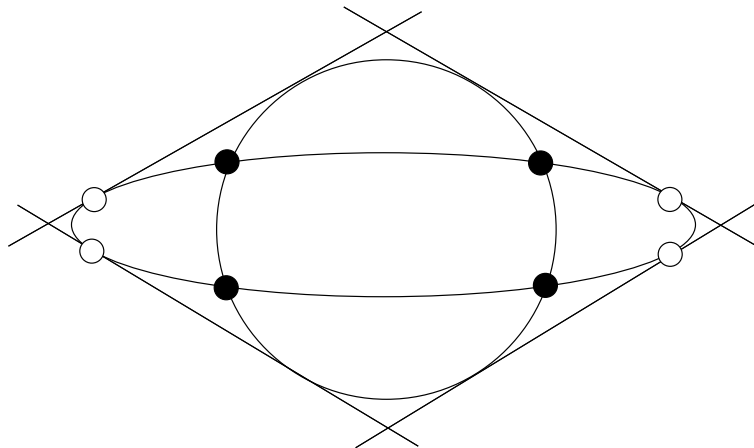


Figure 4: all the branch points

The *singular points* of ϕ_j are the pre-images of the branch points. There are 4 such points. When uniformized, \mathbf{T} is obtained by gluing the opposite sides of a rectangle in the obvious way. Referring to Figure 5, the black points indicate the singular points of ϕ_1 and the white points indicate the singular points of ϕ_2 . Reflection in the vertical centerline swaps black and white points. The dotted horizontal lines are $\phi_1^{-1}(C_1)$. This well-known structure is recalled in my paper on the Poncelet Grid. ²

²Our picture here differs from the one there only in that we are rotating the torus by 90 degrees so as to switch the roles played by horizontal and vertical.

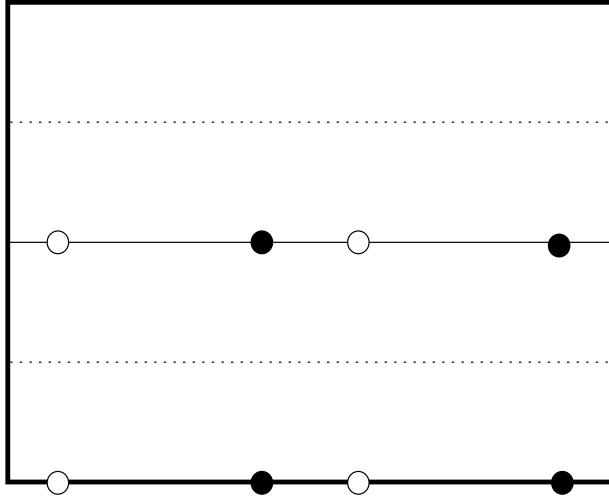


Figure 5: singular points

There is an involution $I_j : \mathcal{T} \rightarrow \mathcal{T}$ that commutes with ϕ_j . The involution I_j fixes the singular points of ϕ_j . The group $D_n = \langle I_1, I_2 \rangle$ is the dihedral group of order $2n$. The map ϕ_1 maps the D_n -orbits to Poncelet polygons. The Poncelet polygon is ordinary iff its image has n points. This happens iff the orbit does not contain one of the singular points of ϕ_1 or ϕ_2 . Thus, there are $4n$ degenerate points. Each degenerate point is equivalent under D_n to one of the singular points. $2n$ of these degenerate points lie on the center horizontal line in Figure 5, hereafter called *the centerline* and denoted by Ξ . The other $2n$ lie on the bottom/top horizontal edge of the rectangle. By symmetry, it suffices to consider the ones on the centerline.

Figure 6 shows the degenerate points arranged along Ξ in case $n = 4$. The endpoints of Ξ are identified, so that Ξ is really a circle. The degenerate points on the Ξ are arranged into two D_n -orbits. One of the orbits consists of the black points and the other orbit consists of the white points. This picture is representative of the even cases n . Referring to Lemma 3.4 we just need to analyze these two special orbits.

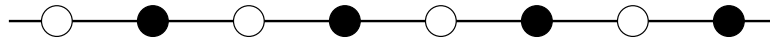


Figure 6: degenerate points on the centerline

For the odd cases, the picture is a bit different, and for convenience we ignore it.

6 Models for the Degenerations

We already mentioned that we only consider the case when n is even. As another convenience, we take n large, say $n > 100$. The purpose of taking n large is so that we can isolate the (two) parts of a degenerate Poncelet polygon that cause us trouble.

Let Ξ denote the centerline of \mathbf{T} . The map $\phi_1 : \Xi \rightarrow C_1$ is a 2-to-1 folding map. The two singular points on Ξ are mapped to the two upper intersection points of $C_1 \cap C_2$, and $\phi_1(\Xi)$ is precisely the uppermost arc of $C_1 - C_2$. Outside any neighborhood U of the two singularities of ϕ_1 , the map ϕ_1 is C_U -bilipschitz. Here C_U depends on the neighborhood U . Here Ξ is given its uniformized metric and C_1 is given its usual metric.

We call the singular orbits on Ξ by Ψ_1 and Ψ_2 . These orbits have the following description.

1. Ψ_1 is the D_n -orbit of the 2-singularities of ϕ_1 that lie on Ξ – the black points in Figure 5. The restriction of ϕ_1 to Ψ_1 is 2-to-1 on all but 2 points of this orbit. the image $\phi_1(\Psi_1)$ consists of $(n/2) + 1$ points.
2. Ψ_2 is the D_n -orbit of the 2-singularities of ϕ_2 that lie on Ξ – the white points in Figure 5. In this case, $\phi_1(\Psi_1)$ maps this orbit to C_1 in a 2-to-1 fashion.

Given the folding nature of ϕ_1 , Figure 7 shows a fairly accurate picture of one end of $\phi_1(\Psi_1)$ and $\phi_1(\Psi_2)$. The other end is the mirror reflection. The points in the middle are not really of interest to us. In the first case, the point labelled 5 is the branch point.

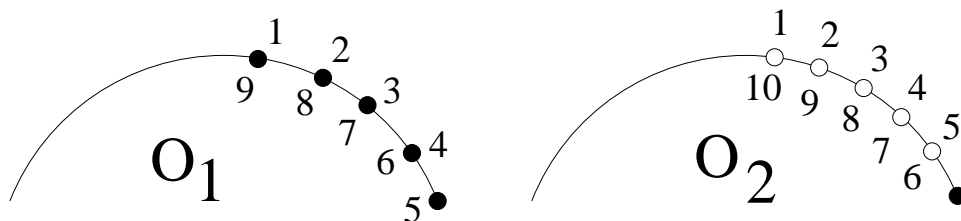


Figure 7: local picture of the degenerate polygons

For small ϵ , the D_n -orbit Ψ_j^ϵ that is ϵ away from Ψ_j is obtained from Ψ_j by replacing each point of Ψ_j by two points, on either side, that are 2ϵ apart. The picture of $\phi_1(\Psi_1^\epsilon)$ corresponding to Figure 7 is obtained by replacing the

points commonly labelled $(1, 9)$ $(2, 8)$, $(3, 7)$ and $(4, 6)$ each by two points that are between $C^{-1}\epsilon$ and $C\epsilon$ apart. Here C is a positive constant that only depends on n . For Ψ_2 the picture is similar, except that all points are split apart. The estimate on the spacing comes from the bi-lipschitz nature of ϕ_1 away from the singularities.

We find it convenient to apply a projective transformation that moves C_1 to the standard parabola

$$\Pi = \{(x, y) \mid y = x^2\} \tag{15}$$

carries the rightmost points in our pictures to $(0, 0)$. Such a projective transformation is bi-lipschitz. To draw pictures in Π , we consider the projection onto the first coordinate. Figure 8 shows a fairly accurate picture of one end of (the renormalized image of) $\phi_1(\Psi_j^\epsilon)$.

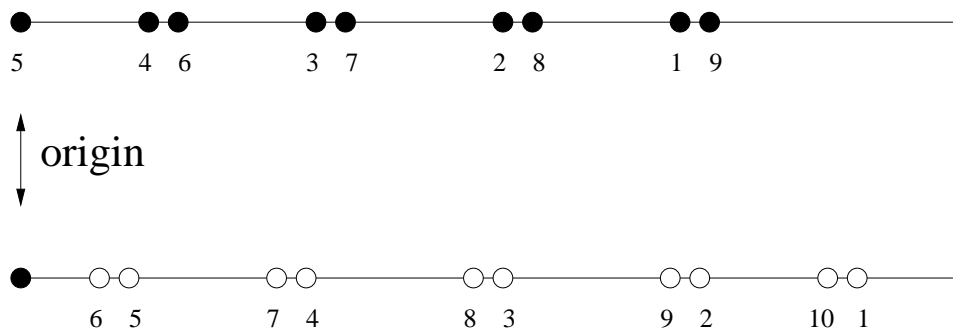


Figure 8: local model of the degenerations

The left endpoint is the origin. The only point we have not justified is the ordering of the points in Figure 8. The order we have drawn follows from the way D_n acts on Ξ . Alternatively, this order can be determined experimentally in one case; then the order remains unchanged in all cases by continuity. Again, we are showing the first coordinates of our points. They really lie on the parabola Π . Whether we consider the points on Π or just the first coordinates, the spacing between nearby points is between $C^{-1}\epsilon$ and $C\epsilon$, and the spacing between all other pairs of points is at least C^{-1} . Here C only depends on n .

Figure 8 gives us our local model for the way the Poncelet polygons degenerate at one end. The other end, halfway around in terms of the ordering on the points, is similar. The points in the middle play little role in the analysis, though sometimes we will have to consider these points in a very general sort of way.

7 Proof of Lemma 3.3

7.1 Reduction to Three Estimates

We refer to the notation used in our model, described in §5. We will just deal with the invariant

$$O_n = \prod_{i=1}^n x_i. \quad (16)$$

The case of E_n is entirely similar and indeed follows from symmetry.

For ease of exposition, we will just consider the orbits Ψ_1^ϵ . The orbits Ψ_2^ϵ have an almost identical treatment. Referring to our model in Figure 6, we just have to show that the product $x_2x_3x_4$ remains bounded as $\epsilon \rightarrow 0$. For other nearby indices, the corner invariants involve 5 points that remain in general position even in the limit. The singularity at the other end has the same analysis.

We use the usual notation $f = O(g)$ to indicate that f/g lies between two positive constants that depend only on n . We will establish 3 estimates for ϵ sufficiently small.

1. $x_2 = O(\epsilon)$.
2. $x_3 = O(1)$.
3. $x_4 = O(1/\epsilon)$.

Combining these estimates, we see that $x_2x_3x_4 = O(1)$. Hence, the product of interest to us remains bounded as $\epsilon \rightarrow 0$.

Our analysis in each case follows the same pattern. We will write

$$x_k = [a, b, c, d] \quad (17)$$

where a, b, c, d depend on both the index k and on ϵ . We will then analyze the geometry of a, b, c, d as $\epsilon \rightarrow 0$.

7.2 The First Estimate

The points of interest to us are shown in Figure 9. The points of interest to us are

$$a = V(2); \quad b = V(3); \quad c = L(23) \cap L(45); \quad d = L(23) \cap L(56).$$

Here $L(23)$ denotes the line through $V(2)$ and $V(3)$, etc. Looking at the picture, and using our model, we see that

$$\|c - d\| = O(\epsilon); \quad \|x - y\| = O(1); \quad x \in \{a, b\} \quad y \in \{c, d\}. \quad (18)$$

Hence $x_2 = O(\epsilon)$.

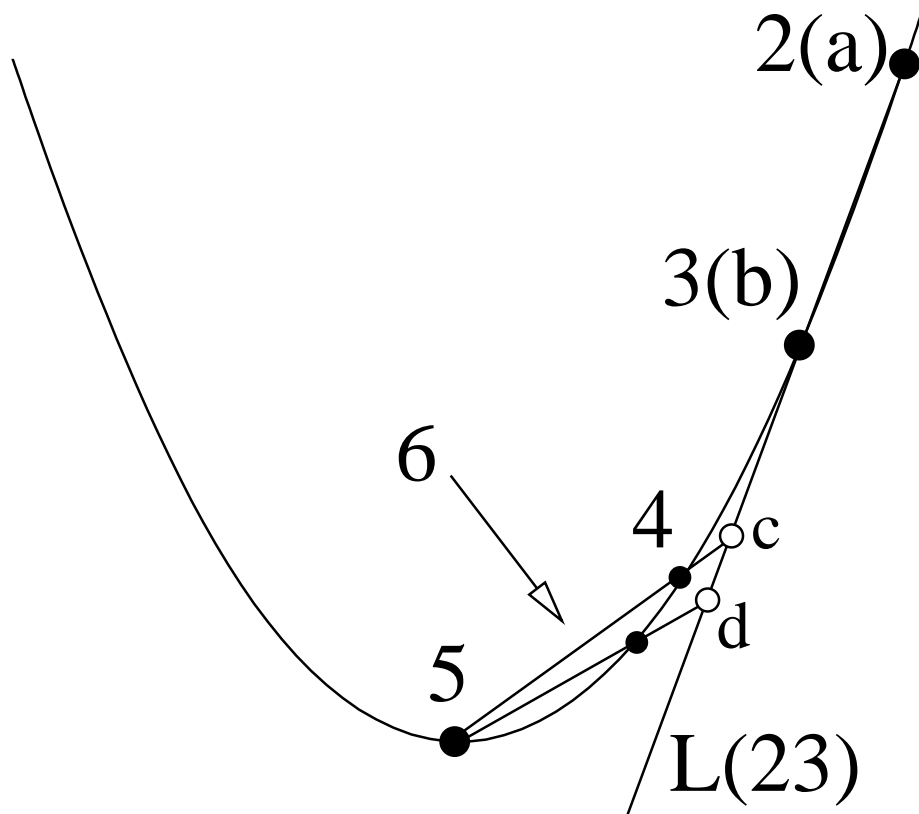


Figure 9: Estimating x_2 .

7.3 The Second Estimate

Figure 10 shows the situation for x_3 . The points of interest to us are

$$a = V(3); \quad b = V(4); \quad c = L(56) \cap L(34); \quad d = L(67) \cap L(34).$$

There is an $O(1)$ -bilipschitz projective transformation that carries the points $V(3), V(7), V(4), V(6)$ to the vertices of a rectangle. (We mean that the transformation is $O(1)$ -bilipschitz on the convex hull of these points.) From this, we conclude that

$$\|d - b\| = O(1); \quad \|d - a\| = O(1).$$

But then $\|d - c\| = O(1)$ as well. Also, $\|a - b\| = O(1)$ and $\|a - c\| = O(1)$. Hence $x_3 = O(1)$.

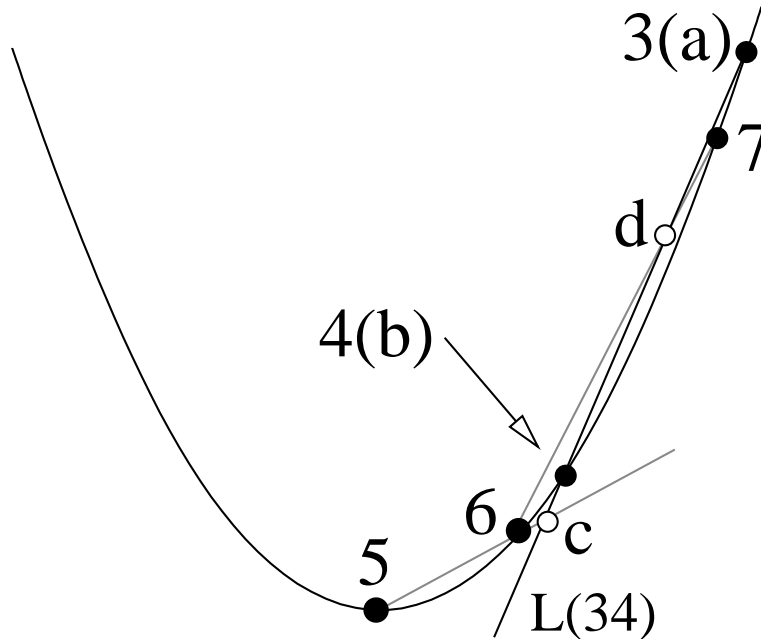


Figure 10: Estimating x_3 .

More is true in this case, since $\|b - c\| = O(\epsilon)$ we conclude that

$$\left| 1 - \frac{\|a - b\|}{\|a - c\|} \right| = O(\epsilon); \quad \left| 1 - \frac{\|d - b\|}{\|d - c\|} \right| = O(\epsilon).$$

From this, we see that

$$\left| 1 - x_3(P^\epsilon) \right| = O(\epsilon). \tag{19}$$

7.4 The Third Estimate

Figure 11 shows the situation for x_4 . The points of interest to us are

$$a = V(4); \quad b = V(5); \quad c = L(67) \cap L(45); \quad d = L(68) \cap L(45).$$

In the same sense as the previous case, there is a uniformly bilipschitz projective map that carries $V(5), V(6), V(4), V(7)$ to a trapezoid whose 3 long sides have length 1 and whose short side has length ϵ . From this, we get

$$\|c - a\| = O(\epsilon). \quad (20)$$

Consider the triangle $(V(4), V(7), d)$. The small angles of this triangle are all $O(1)$. Also, one side of this triangle, namely the one connecting $V(4)$ to $V(7)$, has length $O(1)$. Hence all sides have length $O(1)$. In particular,

$$\|d - a\| = O(1) \quad (21)$$

But then we have $\|c - d\| = O(1)$ and $\|b - d\| = O(1)$. Finally, $\|b - a\| = O(1)$. Hence $x_4 = O(\epsilon^{-1})$.

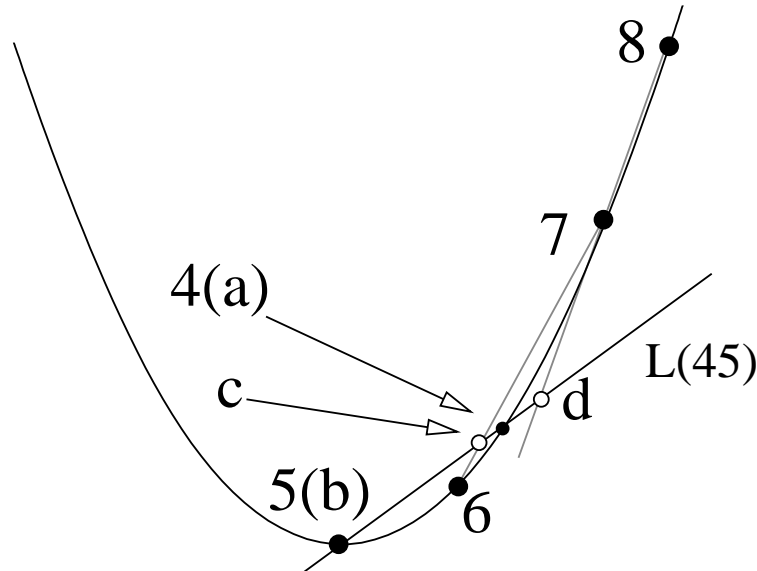


Figure 11: Estimating x_4 .

Putting everything together, and slightly abusing the notation, we have

$$x_2 x_3 x_4 = O(\epsilon) O(1) O(\epsilon^{-1}) = O(1).$$

This completes the proof of Lemma 3.1.

8 Lemma 3.4 Modulo a Detail

We fix some large value of n . As in the proof of Lemma 3.3, we will just deal with the degenerations associated to the orbit Ψ_1 . The proof for the degenerations associated to Ψ_2 is essentially the same.

Let P^ϵ denote the Poncelet polygon associated to the perturbed orbit Ψ_1^ϵ . In constructing P_t^ϵ we normalize so that the vertices labelled 2, 3, 4, 5 are independent of t . Let P denote the degenerate Poncelet polygon corresponding to $\epsilon = 0$. We use our model from Figure 8. The purpose of this section is to prove the following result

Lemma 8.1 (Variation) *Suppose that $\{(\epsilon_n, t_n)\}$ is any sequence converging to $(0, 1)$. Then*

$$V_{t_n}^{\epsilon_n}(k) \rightarrow V(k); \quad k = 6, 7, 8$$

We prove this result in the next section. In the following lemma, we take the indices mod n on the right hand side of the main equation.

Corollary 8.2 *Suppose that $\{(\epsilon_n, t_n)\}$ is any sequence converging to $(0, 1)$. Then*

$$V_{t_n}^{\epsilon_n}(k) \rightarrow V(k); \quad k \geq 6.$$

Proof: Let x_1, y_1, \dots be the corner invariants. To summarize our proof of Lemma 3.3, we showed

$$x_2(P_1^\epsilon) = O(\epsilon); \quad x_4(P_1^\epsilon) = O(\epsilon^{-1}) \quad (22)$$

and $x_k(P_1^\epsilon) = O(1)$ for all nearby k . The same argument shows that

$$y_6(P_1^\epsilon) = O(\epsilon^{-1}); \quad y_8(P_1^\epsilon) = O(\epsilon) \quad (23)$$

and $y_k = O(1)$ for all nearby k . For convenience, we repeat the relevant half of Figure 8.

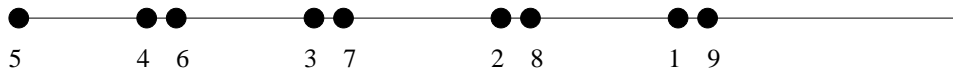


Figure 12: local model of the degeneration

For convenience, we use the notation

$$V_n(k) = V_{t_n}^{\epsilon_n}(k).$$

We focus our attention on the pentagon

$$V_n(5), \dots, V_n(9) \tag{24}$$

From the Variation Lemma and our normalization, which takes care of $V_n(5)$, we see that $V_n(k) \rightarrow V(k)$ for $k = 5, 6, 7, 8$. The pentagon made from $V(k)$ for $k = 5, 6, 7, 8, 9$ is strictly convex, and both $x_5(P^\epsilon)$ and $y_9(P^\epsilon)$ exist, are finite, and are continuous at $\epsilon = 0$. Hence

$$x_5(P_n) \rightarrow x_5(P); \quad y_9(P_n) \rightarrow y_9(P).$$

By Lemma 4.1, we now see that the conclusion of the Variation Lemma holds for $k = 9$.

Now we can repeat this argument, shifting the indices by 1. hence, the conclusion of the Variation Lemma holds for $k = 10$. Continuing in this way, we see that Variation Lemma holds for all $k = 5, \dots, (n/2) + 5$.

We have made our analysis under the assumption that the vertices $V_n(k)$ are fixed, for $k = 2, 3, 4, 5$. However, we would get the same conclusion if these vertices varied in a way such that $V_n(k) \rightarrow V(k)$ for $k = 2, 3, 4, 5$. We could adjust the picture, for each n , by a projective transformation T_n that converges to the identity.

We have established that

$$V_n(k + n/2) \rightarrow V(k + n/2); \quad k = 2, 3, 4, 5$$

Our analysis in the proof of Lemma 3.3 works equally well for the degeneracy corresponding to the index $(n/2) + 5$. We conclude that the Variation Lemma holds when we shift indices by $n/2$. But then we can repeat our argument above. We conclude that the Variation Lemma holds for $k = (n/2) + 6, \dots, n + 5$. Now we can repeat the argument and take care of the next $n/2$ vertices, and so on. ♠

Proof of Lemma 3.4: If Lemma 3.4 is false, then for every $\epsilon > 0$, we can find some t , arbitrarily close to 1, such that P_t^ϵ does not converge to P on the first n vertices. But this contradicts the result we just established. This proves Lemma 3.4 modulo the Variation Lemma. ♠

9 Some Auxilliary Cross Ratios

We need to understand the geometry of some of other cross ratios before making out estimate. We will just consider the case of the variation Ψ_1 . Let $L(ij)$ denote the slope of the line containing $V(i)$ and $V(j)$. Let

$$z_5 = [L(35), L(45), L(65), L(75)]. \quad (25)$$

Normalizing as in Lemma 4.1, we compute that

$$z_5 = x_3 y_7. \quad (26)$$

Let $\{P^\epsilon\}$ be the family of polygons corresponding to the degenerating orbits Ψ_1^ϵ .

Lemma 9.1 $|1 - z_5(P^\epsilon)| < C\epsilon^2$ for some C that only depends on n .

Proof: Let \mathbf{T} denote the complex torus of flags, constructed in §5. We introduce local complex coordinates on \mathbf{T} so that P^z is the Poncelet polygon determined by the point $z \in \mathbf{C}$. We only care about this local coordinate system for $|z|$ sufficiently small. We arrange that $x = \epsilon$ corresponds to P_ϵ . As $\epsilon \rightarrow 0$, the point $V(5)$ converges to a singular point, as in Figure 12. There is a basic symmetry: Rotation about the point of \mathbf{T} corresponding to $z = 0$ carries P^ϵ to $P^{-\epsilon}$ in such a way that the k -th vertex of P^ϵ is mapped to the $10 - k$ th vertex of $P^{-\epsilon}$.

We define $\tau(z) = x_3(P^z)$. From the basic symmetry just mentioned, we get

$$y_7(P^\epsilon) = \tau(-\epsilon).$$

Therefore

$$z_5(P^\epsilon) = \tau(\epsilon)\tau(1 - \epsilon).$$

Equation 19 says that we can write the Taylor series expansion

$$\tau(z) = 1 + C_1 z + C_2 z^2 + \dots$$

Therefore

$$\tau(\epsilon) = 1 + C_1 \epsilon + C_2 \epsilon^2 \dots; \quad \tau(-\epsilon) = 1 - C_1 \epsilon + C_2 \epsilon^2 \dots$$

Multiplying these two expressions, the coefficient of ϵ cancels, and we get

$$\tau(\epsilon)\tau(-\epsilon) = 1 + C'_2 \epsilon^2 + C'_3 \epsilon^3 \dots$$

This proves what we want. ♠

10 Proof of the Variation Lemma

10.1 The First Estimate

We treat the case $k = 6$ of the Variation Lemma. We use the invariants z_1, z_2, \dots introduced in the previous section. First of all, we have

$$z_4(P_n) = z_4(P_{t_n}^{z_n}) = z_4(P^{z_n}). \quad (27)$$

The first equality is just a definition. The second equality comes from Equation 8 and Equation 26.

It follows from Equation 27 that

$$L_n(46) \rightarrow L(46). \quad (28)$$

Here $L_n(46)$ is the line through $V_n(4)$ and $V_n(6)$ and $L(46)$ is the tangent line to the parabola Π at $V(4) = V(6)$. Referring to Figure 13, the points c_n and d_n depend on n . From Estimate 1 in the proof of Lemma 3.3, we have $x_2(P_n) = O(\epsilon_n)$. Hence

$$\frac{\|V_n(6) - V(6)\|}{\|V(6) - V(4)\|} \rightarrow 0 \quad \|V_n(6) - V(4)\| = O(\epsilon_n). \quad (29)$$

The first equation implies the second. The second restates the Variation Lemma for $k = 6$.

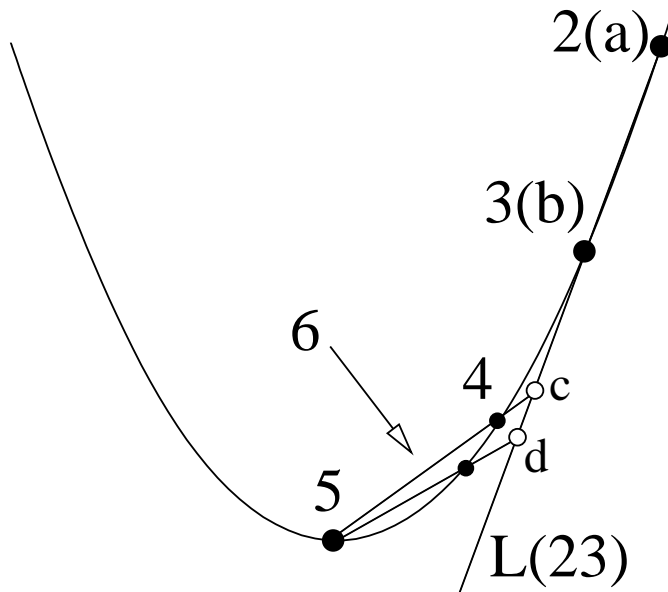


Figure 13: The relevant points.

10.2 The Second Estimate

Now we consider the case $k = 7$ of the Variation Lemma. We will establish two results.

1. As $n \rightarrow \infty$, the line $L_n(67)$ converge to the line $L(67)$.
2. As $n \rightarrow \infty$, the line $L_n(57)$ converge to the line $L(57)$.

Since the limiting lines have different slopes, and intersect only at $V(7)$, these two results combine to say that $V_n(7) \rightarrow V(7)$.

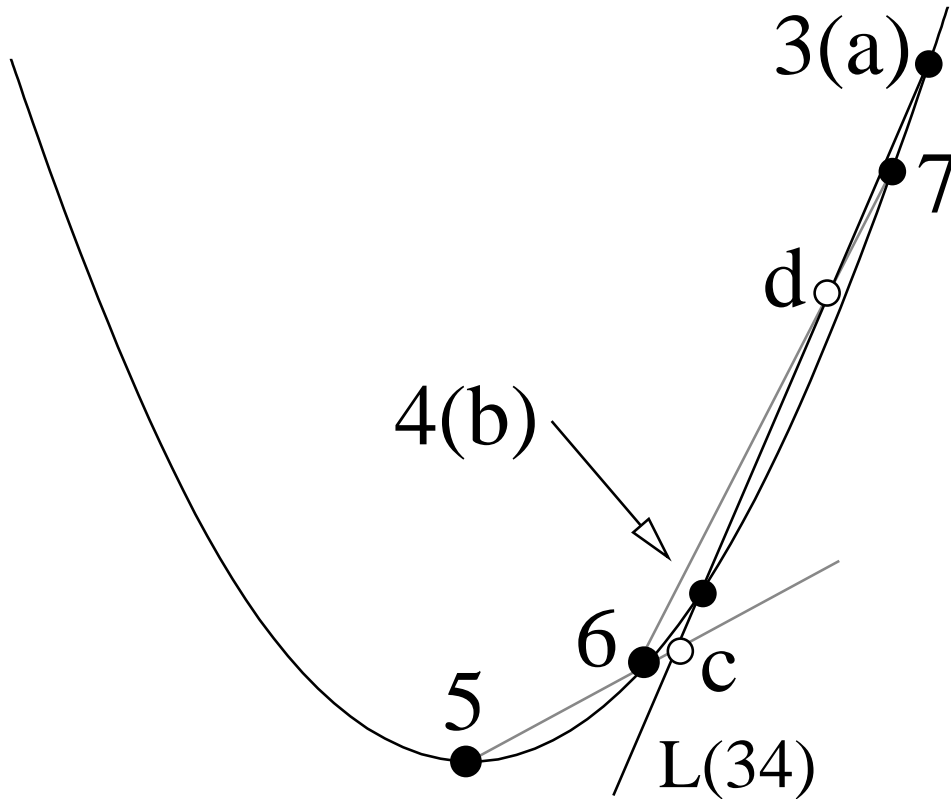


Figure 14: The relevant points

The first statement above uses Figure 10, which we repeat here as Figure 14. From our analysis of the case $k = 6$, we get

$$\|V_n(6) - V(4)\| = O(\epsilon_n); \quad L_n(64) \rightarrow L(64); \quad L_n(63) \rightarrow L(63). \quad (30)$$

Suppose that $L_n(67) \not\rightarrow L(67)$. Passing to a subsequence, we can assume

$$\text{angle}\left(L_n(67), L_n(63)\right) > C$$

But, referring to Figure 14, this big angle combines with Equation 30 to give

$$\|d - c\| = O(\epsilon_n)$$

But then $x_3(P_n)$ does not converge to 1. This contradicts Equation 19.

The second statement also uses Figure 14. It follows from our analysis in the case $k = 6$ that

$$\text{angle}\left(L_n(45), L_n(56)\right) = O(\epsilon_n). \quad (31)$$

The first of these lines is independent of n . Suppose that $L_n(57) \not\rightarrow L(57)$. Passing to a subsequence, we can assume

$$\text{angle}\left(L_n(57), L_n(53)\right) > C$$

But then

$$|1 - z_5(P_n)| > C\epsilon_n,$$

contradicting Lemma 9.1.

10.3 The Third Estimate

Now we consider the case $k = 8$ of the Variation Lemma. We will establish two results.

1. As $n \rightarrow \infty$, the line $L_n(68)$ converge to the line $L(68)$.
2. As $n \rightarrow \infty$, the line $L_n(78)$ converge to the line $L(78)$.

Since the limiting lines have different slopes, and intersect only at $V(8)$, these two results combine to say that $V_n(8) \rightarrow V(8)$.

Our arguments refer to Figure 11, which we reproduce here as Figure 15.

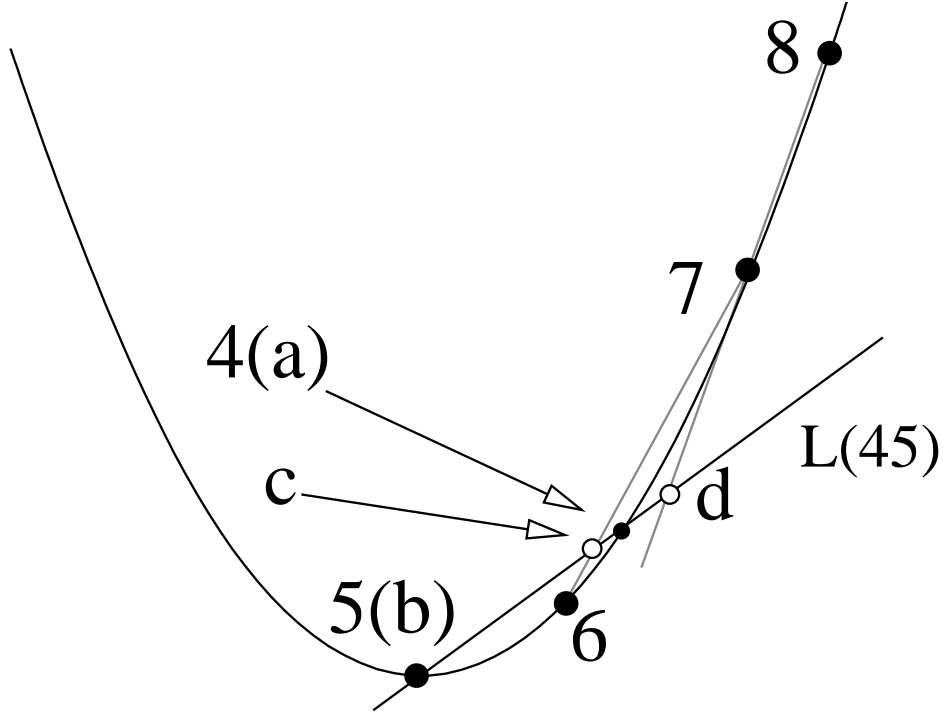


Figure 15: The relevant points

For the first statement, note that $z_6(P)$ exists because the lines $L(6k)$ are distinct for $k = 4, 5, 7, 8$. Moreover,

$$z_6(P_n) \Rightarrow z_6(P); \quad L_n(6k) \rightarrow L(6k); \quad k = 4, 5, 7. \quad (32)$$

This forces $L_n(68) \rightarrow L(68)$.

The last estimate is delicate. We consider the cross ratio $x_4(P_n)$. This is the cross ratio of the 4 points a, b, c, d shown in Figure 15. In Figure 15, the points a and b are independent of n and $c = c_n$ and $d = d_n$ depend on n . To show that $L_n(78) \rightarrow L(78)$ it suffices to show that $d_n \rightarrow d$. We introduce the auxilliary points

$$c'_n = c(P^{\epsilon_n}); \quad d'_n = d(P^{\epsilon_n}). \quad (33)$$

That is, we reconsider the picture when t_n is replaced by 1. Since $d'_n \rightarrow d$, it suffices to prove that

$$\left(\frac{\|d_n - b\|}{\|d_n - c\|} \right) / \left(\frac{\|d'_n - b\|}{\|d'_n - c\|} \right) \rightarrow 0. \quad (34)$$

Since $t_n \rightarrow 1$, we have

$$\frac{x_4(P^{\epsilon_n})}{x_4(P_n)} \rightarrow 1. \quad (35)$$

Recalling the definition of these invariants, and recalling that a and b are independent of n , we see that Equation 34 is equivalent to the statement that

$$\frac{\|c_n - a\|}{\|c'_n - a\|} \rightarrow 1. \quad (36)$$

This last equation follows from elementary geometry and three basic facts.

1. $L(45)$ and $L(67)$ are not parallel.
2. Letting $V'_n(7)$ denote Vertex 7 for P^{ϵ_n} , we have

$$\frac{\|V'_n(7) - V_n(7)\|}{\|V_n(7) - V_n(4)\|} \rightarrow 0.$$

- 3.

$$\frac{\|V'_n(6) - V_n(6)\|}{\|V_n(6) - V_n(4)\|} \rightarrow 0.$$

This completes our proof.

11 References

[M] Th. Motzkin, *The Pentagon in the projective plane, and a comment on Napier's rule*, B.A.M.S. **52** (1945) 985-989

[OST] V. Ovsienko, R. E. Schwartz, S. Tabachnikov, *The Pentagon Map: A Discrete Integrable System*, math arxiv:0901.1585 (2008)

[S1] R. Schwartz, *The Pentagon Map*
Journal of Experimental Mathematics **1** (1992) pp. 85-90

[S2] R. Schwartz, *Recurrence of the Pentagon Map*,
Journal of Experimental Mathematics (2001) **186**, pp 105-154

[S3] R. Schwartz, *Discrete Monodromy, Pentagrams, and the Method of Condensation*,
Journal of Fixed Point Theory and Applications **3** (2008) **186**, pp 105-154